ACS Energy LETTERS

http://pubs.acs.org/journal/aelccp

High-Energy All-Solid-State Organic–Lithium Batteries Based on Ceramic Electrolytes

Fang Hao,[‖] Yanliang Liang,[‖] Ye Zhang, Zhaoyang Chen, Jibo Zhang, Qing Ai, Hua Guo, Zheng Fan, Jun Lou, and Yan Yao*

Cite This: *ACS Energy Lett.* 2021, 6, 201–207

Read Online

ACCESS | Metrics & More | Article Recommendations | Supporting Information

ABSTRACT: **Recent studies have identified unique properties of organic battery electrode materials such as moderate redox potentials and mechanical softness which are uniquely beneficial for all-solid-state batteries based on ceramic electrolytes. Here, we further explore the promise of organic materials and demonstrate a sulfide electrolyte-based organic-lithium battery with a specific energy of 828 Wh kg^{-1}, rivaling the state-of-the-art of all-solid-state batteries. Two innovation steps are responsible for the accomplishment. First, the combination of lithium anode and the high-capacity cathode material pyrene-4,5,9,10-tetraone ensures a high theoretical specific energy. Second, the microstructure of the organic cathode is optimized with the introduction of cryomilling, a technique common to processing soft materials but not familiar to electrode fabrication. The cathode material utilization increases to 99.5% as a result, up from the 55–89% previously reported for ceramic electrolyte-based solid-state organic batteries. The improvement highlights the special requirements of solid-state organic electrodes for microstructural engineering while preserving the chemical integrity of components.**

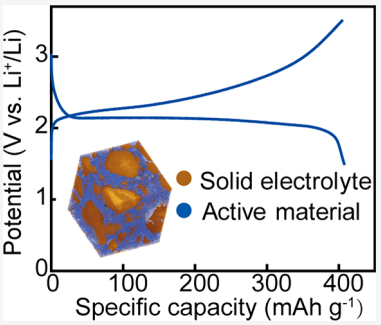

The race to safer and higher-energy batteries is prompting a transition from the liquid electrolyte-based lithium-ion batteries (LIBs) to all-solid-state lithium batteries (ASSLBs), especially those based on ceramic electrolytes.[1−4] Leading candidates of cathode materials for high-energy ASSLBs are those established for LIBs such as $LiNi_{1-x-y}Mn_xCo_yO_2$ (NMC) and sulfur.[5,6] Some of the challenges associated with these materials in LIBs such as electrolyte oxidation at high potentials (NMC) and large volume change (sulfur) become more challenging in ASSLBs, because most ceramic electrolytes have limited anodic stability and are unforgiving of volume change.[7,8] Organic battery electrode materials (OBEMs) may provide a good alternative in this highly competitive field. OBEMs are organic compounds with well-understood redox-active functional groups that reversibly store/release multiple electrons and cations per molecule via an insertion reaction.[9,10] Figure 1a compares the voltage and specific capacity of OBEM-Li, NMC-Li, and sulfur-Li.[11] Structurally simple carbonyl-based OBEMs have redox potentials of 2.0–3.0 V vs Li and specific capacities of 350–590 mAh g^{-1}, both of which are between those of NMC and sulfur. Despite very different voltage and capacity parameters, all three chemistries have the potential to deliver active material-level specific energies of 1000 Wh kg^{-1} or higher.

A semiquantitative comparison of various practical attributes reveals the underlying strengths and weaknesses of OBEMs among the three cathode materials (Figure 1b). While OBEMs do not top the specific energy and energy density departments, they do not have glaring disadvantages in material abundance and electronic/ionic conductivity either.[12,13] Some of the properties that make OBEMs particularly suitable for ASSLBs include moderate redox potential, mechanical softness (and thus formability), and relatively small volume change during cycling.[11,14] Such properties help prevent irreversible deterioration of the cathode material–electrolyte interface, which is often resulted from (electro)chemical reactions at high potentials and particle detachment.[15] As a result, OBEMs have enabled some of the most stable all-solid-state sodium batteries that are based on ceramic electrolytes.[16]

Despite the favorable properties, demonstration of ceramic electrolyte-based solid-state batteries with OBEMs is rare, and high energy is yet to be achieved. The first demonstration of ceramic electrolyte-based organic batteries used a sodium rhodizonate cathode which has a relatively low theoretical specific capacity of 205 mAh g^{-1}.[17] A later study of organic ASSLBs used a carboxylated azo compound with a slightly

Received: October 18, 2020
Accepted: December 10, 2020

https://dx.doi.org/10.1021/acsenergylett.0c02227
ACS Energy Lett. 2021, 6, 201–207

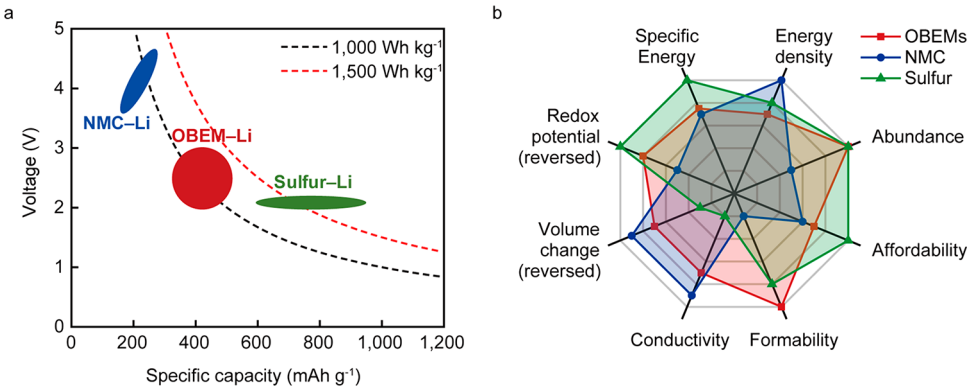

Figure 1. Comparison of OBEMs, NMC, and sulfur as cathode materials for ceramic electrolyte-based batteries. (a) The voltages and specific capacities of lithium batteries based on the three materials. (b) Semiquantitative comparison of practical attributes of the three materials.

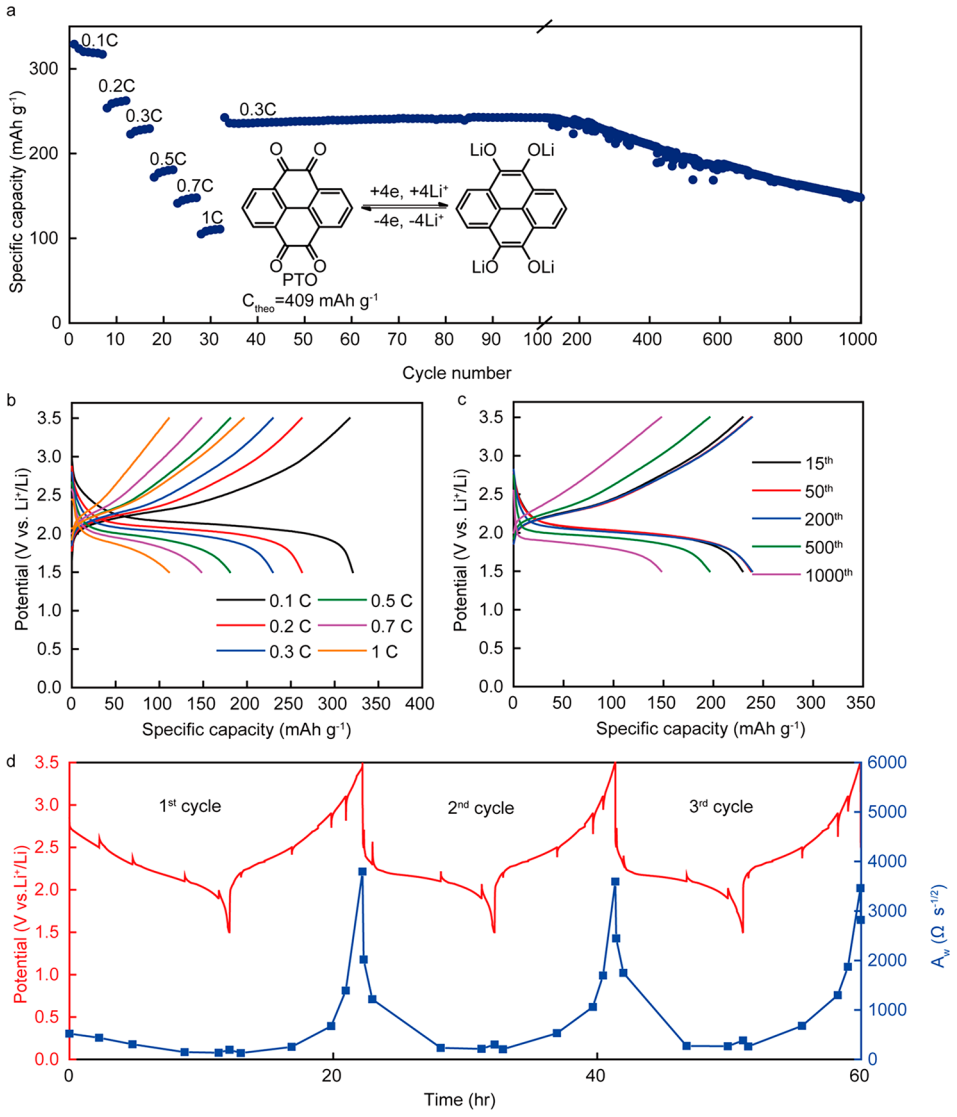

Figure 2. Electrochemical performance of PTO/β-Li_3PS_4/Li cells containing hand-milled PTO/Li_3PS_4/carbon composite cathode at 60 °C (1C = 409 mA g^{-1}). (a) Rate capability and long-term cycling. Inset shows the molecular structure of PTO and its electrochemical reaction. (b) Galvanostatic voltage profile at different current densities, and (c) galvanostatic voltage profile at 0.3C. (d) Warburg coefficient (A_w) at different states of charge and voltage profiles during the initial three cycles at 0.1C.

higher theoretical specific capacity of 231 mAh g^{-1} but poor material utilization of 55%.[18] Attempts toward high specific energy have prompted the use of pyrene-4,5,9,10-tetraone (PTO), which has a theoretical specific capacity of 409 mAh g^{-1}, and a series of optimizations in the conductive agent content and active particle size increased utilization to 79% at a

https://dx.doi.org/10.1021/acsenergylett.0c02227
ACS Energy Lett. 2021, 6, 201−207

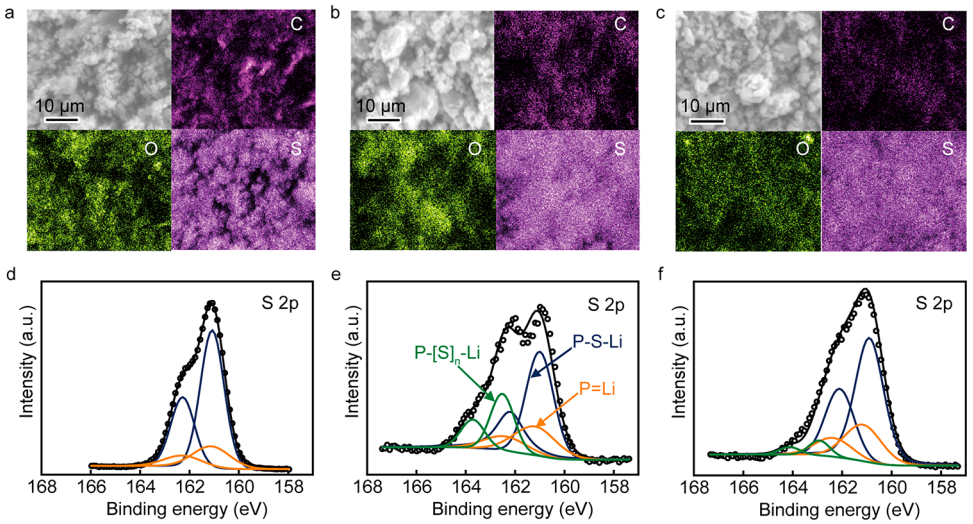

Figure 3. Elemental mapping (a–c) and XPS spectra (d–f) of (a, d) hand-milled, (b, e) ball-milled, and (c, f) cryomilled composites of PTO, β-Li_3PS_4, and carbon.

reasonable rate of $C/10$.[16] This optimized utilization is still significantly lower than that observed in liquid electrolytes, where the utilization of PTO reaches unity.[19] Along with a Na–Sn anode, the resulted specific energy was limited to a middling 400 Wh kg^{-1}.[16] These earlier examples contrast with polymer electrolyte-based organic batteries where high material utilization and high energy are apparently achieved without dedicated microstructural engineering, indicating a challenge specific to ceramic electrolytes (Table S1).[20,21]

Here, we report a ceramic electrolyte-based organic-lithium battery with a state-of-the-art specific energy of 828 Wh kg^{-1}. The combination of PTO cathode and lithium anode ensures a high theoretical cell capacity. The moderate redox potential of PTO maintains a dynamically stable cathode–electrolyte interface, as monitored by electrochemical impedance spectroscopy (EIS). The initially moderate cathode material utilization, 78%, is improved to 99.5% after experimenting with different milling methods. Ball-milling, a common method to homogenize solid-state cathode composites, manages to downsize the electrolyte β-Li_3PS_4 but causes PTO to agglomerate and severely react with Li_3PS_4. Meanwhile, cryomilling scales down both Li_3PS_4 and PTO while suppressing reaction between the two. Conductivity characterizations of the composite cathodes confirm that the domain size reduction of PTO, rather than that of Li_3PS_4 or a more efficient charge transport network, is responsible for the improvement.

ASSLBs with a configuration of PTO-Li_3PS_4/Li_3PS_4/Li were assembled. The electrode reaction of PTO is shown in Figure 2a: upon discharge, each molecule undergoes a four-electron reduction along with 4 Li^+ inserting into the molecular crystal and coordinating with the oxygen atoms. The reaction corresponds to a theoretical specific capacity of 409 mAh g^{-1}. Glass-ceramic β-Li_3PS_4 was selected due to the demonstrated stability of Li_3PS_4 with a lithium anode.[22] For a preliminary study, the cathode composite was prepared by mixing PTO, β-Li_3PS_4, and carbon at a mass ratio of 20:70:10 wt % with a pestle and mortar (hand-milled method), followed by uniaxial powder compaction. The PTO-Li cell exhibits a discharge plateau at 2.2 V with a specific capacity of 318 mAh g^{-1} at $C/10$, corresponding to a material utilization of 78% (Figure 2a). This result is in line with that observed for solid-state PTO-Na cells where a utilization of 79% was recorded[16] and lower than the 88% in a liquid electrolyte despite partial dissolution for the latter.[19] At higher C rates, e.g., $C/2$ and $1C$, specific capacity decreases to 180 and 110 mAh g^{-1}, respectively (Figure 2b). The cell cycles stably at $0.3C$ for the initial 200 cycles and maintains 61% of its maximum capacity at the same C rate after 1000 cycles. The voltage profiles for selected cycles show minimum change, indicating well reversible electrode reactions and minimal irreversible changes in the interfaces (Figure 2c).

The evolution of the cathode–electrolyte interface was probed by in situ EIS (Figure S1). The Warburg coefficient (A_w) extracted from spectra reflects the ionic diffusion resistance at the cathode active material–electrolyte interface.[23] The evolution of A_w in the first three cycles is plotted in Figure 2d. A_w remains low during the majority of a cycle but increases sharply to >1000 $\Omega\ s^{-1/2}$ when the voltage exceeds 2.9 V vs Li^+/Li, at which potential the oxidation of β-Li_3PS_4 is expected.[24,25] Upon discharge, A_w quickly reverts to low values and remains so until charged to high potentials again. The same evolution repeats in the following cycles. A similar reversible increase of A_w was observed for PTO-Na_3PS_4/Na_3PS_4/$Na_{15}Sn_4$ cells, and characterizations of the composite cathode by X-ray photoelectron spectroscopy and time-of-flight secondary ion mass spectrometry suggest that part of the Na_3PS_4 electrolyte within the cathode was reversibly oxidized into species like $Na_2P_2S_6$ and $Na_4P_2S_8$.[16] Considering the similarity between Li_3PS_4 and Na_3PS_4 and the highly familiar evolution of A_w, a reversible oxidation of Li_3PS_4 at the PTO-Li_3PS_4 interface is likely. This reversibility contrasts with the irreversible increase of interfacial resistance observed for layered oxide–sulfide electrolyte composite cathodes.[26–28] The moderate working potential of PTO is responsible for the prevention of irreversible electrolyte oxidation and thus long cycle life.

We went on to address the moderate active material utilization. As summarized earlier, the utilization of organic electrode materials in ceramic electrolyte-based cells has always been relatively low. Our previous studies showed that downsizing the PTO particles to the nanoscale improves rate capability but not utilization.[16] We hypothesized that not only particle size but also microstructure of the composite cathode

https://dx.doi.org/10.1021/acsenergylett.0c02227
ACS Energy Lett. 2021, 6, 201–207

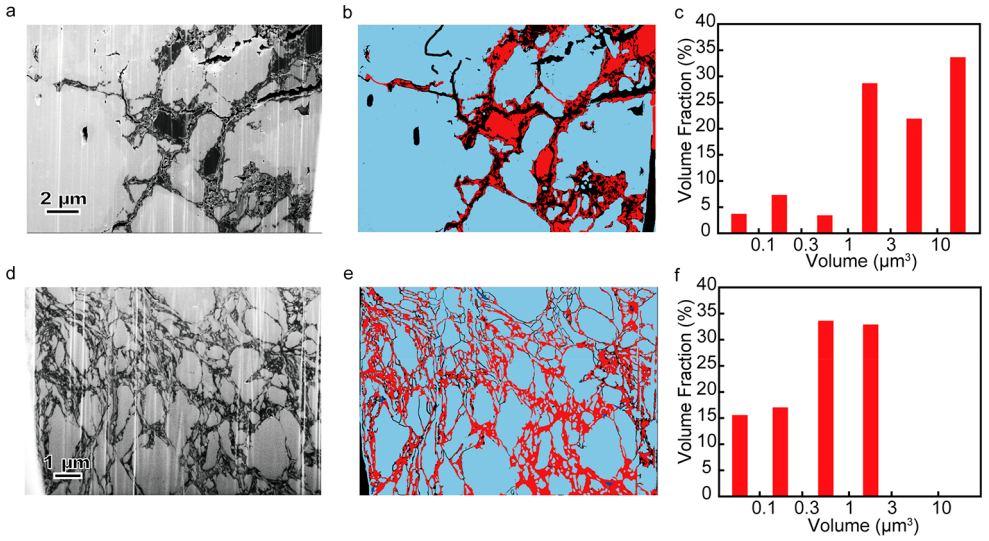

Figure 4. Cross-section analyses of compacted cathodes made with hand-milled (a–c) and cryomilled (d–f) composites. (a, d) SEM images. (b, e) Segmented binary images via thresholding (red, PTO; blue, Li_3PS_4). (c, f) Volume fraction distribution of PTO domains.

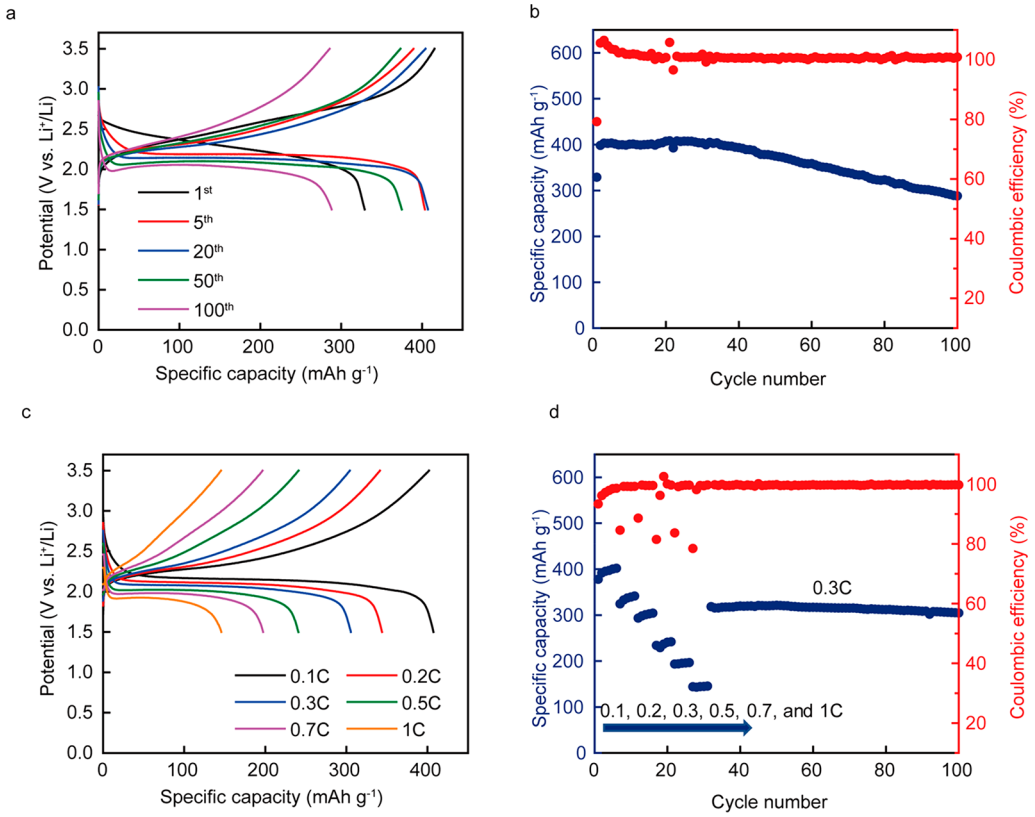

Figure 5. Cell performance of a PTO-Li_3PS_4/Li_3PS_4/Li cell with a cryomilled cathode. (a) Galvanostatic voltage profile at C/10 at the first, fifth, 20th, 50th, and 100th cycles. (b) Capacity retention for 100 cycles. (c) Galvanostatic voltage profiles at different current densities (1C = 409 mA g^{-1}). (d) Rate capabilities.

plays a role in the electrode performance. To verify the hypothesis, we first examined the particle dispersion of the hand-milled powder mixture under scanning electron microscopy (SEM) and energy dispersive spectroscopy (EDS) mapping. All the elements examined segregate into multi-micron-sized domains, indicating agglomeration of both PTO and Li_3PS_4 (Figure 3a). Ball-milling is commonly used in solid-state cathode preparation to simultaneously downsize the materials and homogenize their distribution.[29] We have therefore subjected the PTO-Li_3PS_4-carbon mixture to ball-milling. The distribution of Li_3PS_4 becomes uniform, as expected, but the aggregation of PTO remains (Figure 3b). It is not uncommon that organic compounds are not effectively downsized by milling at ambient or elevated temperature because ductile plastic particles tend to deform and stick together instead of breaking down upon mechanical impact. Even worse, severe oxidation of Li_3PS_4 was detected by X-ray photoelectron spectroscopy (XPS; Figure 3d and e), echoing

https://dx.doi.org/10.1021/acsenergylett.0c02227
ACS Energy Lett. 2021, 6, 201–207

the electrochemical oxidation observed during charging at high potentials. The ASSLB with the ball-milled composite shows low initial Coulombic efficiency and fast capacity decay (Figure S2). Therefore, we need an alternative mixing method that downsizes organics while not causing chemical reactions.

The cryomilling technique is effective in milling soft and ductile materials because such materials go through ductile-to-brittle transition when cooled to liquid-nitrogen temperature. It has long been used for processing polymer samples and preparing nanoscale metallic materials.[30,31] PTO is a soft material with an elastic modulus of 4.2 GPa and does need to be rendered brittle at low temperatures for effective size reduction without aggregation.[16] Figure 3c shows that after cryomilling, both PTO and Li_3PS_4 show relatively uniform distribution. XPS reveals limited reaction between the two components (Figure 3f). The new peaks (green) in the spectrum show similarities with those reported for sulfide-based electrolytes in electrodes at the charged and cycled states,[16,26] and it is reasonable to expect the reaction products share similar composition and reversibility. These results show that cryomilling is a powerful tool for preparing organic electrodes.

The uniform distribution of materials within a composite electrode may enhance electrochemical performance in multiple ways. The uniform distribution of solid electrolyte alone would form a better connected ionic transport network that could improve performance on all fronts.[32−34] Further homogenized distribution of the active material would enable faster charge transport within the active material and more efficient charge transfer between the active material and the electrolyte.[35,36] To probe the importance of each step, we measured the conductivity of both the electrodes made from hand-milled and cryomilled powders. EIS of Cu/PTO-Li_3PS_4/Cu cells was performed in the temperature range of 25−100 °C, and the conductivity values were extracted by fitting the Nyquist plot following a procedure reported for mixed electronic−ionic conductors (Figure S3).[37] The two samples show almost identical electronic and ionic conductivities. Therefore, the improvement in distribution of the electrolyte alone is not enough to provide expectable performance of the PTO-Li_3PS_4 electrode. The cryomilling and the resulted downsizing of PTO domains are essential to introducing a material difference in performance.

The size of PTO domains in various compacted PTO-Li_3PS_4-carbon electrodes is quantified via analysis of the intersection. The SEM images in Figure 4a and d show that the PTO domains in both the hand-milled and cryomilled samples are squeezed into irregular shapes, the sizes of which could not be quantified by the direct measurement of their dimensions. We have therefore segmented the SEM images based on greyscale thresholds and identified the PTO domains as computer-analyzable binary images (Figure 4b and e). The images were then statistically analyzed and the area fraction of domain sizes was converted into volume fraction. The size of PTO domains in the electrode made from cryomilled powders is on average 1 order of magnitude smaller than that from hand-milled ones (Figure 4c and f). Such significant reduction in the size of the active material has been widely reported to contribute to improved battery performances.[38,39]

ASSLBs based on electrodes made from cryomilled composites deliver specific capacities of up to 407 mAh g^{-1}, corresponding to a material utilization of 99.5% (Figure 5a). This is the first time an organic electrode material accomplishes full utilization in a ceramic electrolyte-based battery. The material-level specific energy of 828 Wh kg^{-1}, based on the weight of Li_4PTO, puts the battery up among the best solid-state chemistries and shows the potential of OBEMs in enabling high-energy batteries. The first discharge capacity is low due to the partial reduction (even though largely suppressed) of PTO by β-Li_3PS_4 during cryomilling, confirming the observation from XPS spectra. Attempts to increase the ratio of PTO in the cathode composite to 40 and 60 wt % were met with decreased utilization (Figure S4), reflecting an ongoing challenge for high-capacity cathode materials (e.g., sulfur) for all-solid-state batteries.

The specific capacity reaches ∼400 mAh g^{-1} as early as the first charge and stays stable for ∼30 cycles at full utilization, then starts to decay steadily and drops to 288 mAh g^{-1} after 100 cycles (Figure 5b). Polarization also increases slightly over the cycles. These patterns of evolution are similar to those observed for electrodes made from hand-milled powders. It is not clear at this stage whether the PTO cathode or the lithium anode is responsible for the polarization buildup and gradual capacity decay, and the mechanism(s) behind these evolutions. A possible failure mechanism for the cathode is that even though PTO's moderate potential allows for a largely reversible interface evolution, some small fraction of the reacted electrolyte may not fully recover, and the accumulation of this fraction gets faster when the contact area between the active material and the electrolyte increases. Therefore, while the capacity decay only slowly kicks in after 200 cycles for the electrode made from a hand-milled composite, it comes much earlier for the electrode made with a cryomilled composite. An indirect confirmation of this hypothesis comes from the cycling performance of the cryomilled composite at 0.3*C* (Figure 3c and d). The cell cycles stably at 0.3*C*, maintaining ∼100% of its maximum capacity at the same *C* rate after 100 cycles. The much increased stability over the same number of cycles but much shorter time duration implies that the capacity decay observed at 0.1*C* is not due to structural failures (contact failure, particle pulverization, lattice distortion, etc.), which correlates with cycle number, but relates to interfacial chemical side reactions, which correlates with reaction time. Comprehensive characterization tools are being developed in our lab for in-depth understanding and potential improvements.

In summary, we have demonstrated a high-energy ASSLB using a PTO-β-Li_3PS_4 organic cathode. By introduction of the cryomilling technique, the organic material PTO is downsized and homogenized with the electrolyte without undergoing significant chemical reaction. A record-high material utilization is achieved as a result. The successful integration of a high-capacity OBEM into an actively pursued ceramic electrolyte-based solid-state battery without sacrificing material utilization opens an alternative path toward high-energy batteries, an area currently dominated by literally two cathode materials. The plausibility to use OBEMs in ASSLBs brings many new possibilities to the technology due to their unique feature set of material availability, mechanical properties, electrode reaction characteristics, etc. Multidimensional diagnostic techniques, optimized fabrication methods, and new OBEMs and are being developed for further performance improvement.

■ ASSOCIATED CONTENT

Supporting Information

The Supporting Information is available free of charge at https://pubs.acs.org/doi/10.1021/acsenergylett.0c02227.

https://dx.doi.org/10.1021/acsenergylett.0c02227
ACS Energy Lett. 2021, 6, 201−207

Experimental methods, electrochemical performance data, EIS spectra, and conductivities measurements (PDF)

AUTHOR INFORMATION

Corresponding Author

Yan Yao − *Department of Electrical and Computer Engineering and Texas Center for Superconductivity at the University of Houston (TcSUH), University of Houston, Houston, Texas 77204, United States;* orcid.org/0000-0002-8785-5030; Email: yyao4@uh.edu

Authors

Fang Hao − *Department of Electrical and Computer Engineering and Texas Center for Superconductivity at the University of Houston (TcSUH), University of Houston, Houston, Texas 77204, United States;* orcid.org/0000-0002-7701-6874

Yanliang Liang − *Department of Electrical and Computer Engineering and Texas Center for Superconductivity at the University of Houston (TcSUH), University of Houston, Houston, Texas 77204, United States;* orcid.org/0000-0001-6771-5172

Ye Zhang − *Department of Electrical and Computer Engineering and Texas Center for Superconductivity at the University of Houston (TcSUH), University of Houston, Houston, Texas 77204, United States*

Zhaoyang Chen − *Department of Electrical and Computer Engineering and Texas Center for Superconductivity at the University of Houston (TcSUH), University of Houston, Houston, Texas 77204, United States*

Jibo Zhang − *Department of Electrical and Computer Engineering and Texas Center for Superconductivity at the University of Houston (TcSUH), University of Houston, Houston, Texas 77204, United States*

Qing Ai − *Department of Materials Science and NanoEngineering, Rice University, Houston, Texas 77005, United States*

Hua Guo − *Department of Materials Science and NanoEngineering, Rice University, Houston, Texas 77005, United States*

Zheng Fan − *Department of Engineering Technology, University of Houston, Houston, Texas 77204, United States*

Jun Lou − *Department of Materials Science and NanoEngineering, Rice University, Houston, Texas 77005, United States;* orcid.org/0000-0002-4351-9561

Complete contact information is available at: https://pubs.acs.org/10.1021/acsenergylett.0c02227

Author Contributions

‖F.H. and Y.L. contributed equally.

Notes

The authors declare the following competing financial interest(s): Y.Y. has an equity interest in Polymax Energy Inc. Y.Y.s relationship with Polymax Energy Inc. has been reviewed and approved by the University of Houston in accordance with its conflict of interest policies.

ACKNOWLEDGMENTS

The work was mainly support by the U.S. Department of Energy's Office of Energy Efficiency and Renewable Energy (EERE), as part of the Battery 500 Consortium under contract DE-EE0008234. The work on cross-section characterization and image analysis was supported by the U.S. Department of Energy's Office of Energy Efficiency and Renewable Energy (EERE) under the Vehicle Technologies Program under Contact DE-EE0008864. We appreciate Prof. Jiming Bao for the use of a cryogenic grinder.

REFERENCES

(1) Randau, S.; Weber, D. A.; Kötz, O.; Koerver, R.; Braun, P.; Weber, A.; Ivers-Tiffée, E.; Adermann, T.; Kulisch, J.; Zeier, W. G.; Richter, F. H.; Janek, J. Benchmarking the Performance of All-Solid-State Lithium Batteries. *Nat. Energy* **2020**, *5*, 259−270.

(2) Manthiram, A.; Yu, X.; Wang, S. Lithium Battery Chemistries Enabled by Solid-State Electrolytes. *Nat. Rev. Mater.* **2017**, *2*, 16103.

(3) Chen, R.; Li, Q.; Yu, X.; Chen, L.; Li, H. Approaching Practically Accessible Solid-State Batteries: Stability Issues Related to Solid Electrolytes and Interfaces. *Chem. Rev.* **2020**, *120*, 6820−6877.

(4) Sun, C.; Liu, J.; Gong, Y.; Wilkinson, D. P.; Zhang, J. Recent Advances in All-Solid-State Rechargeable Lithium Batteries. *Nano Energy* **2017**, *33*, 363−386.

(5) Lee, Y.-G.; Fujiki, S.; Jung, C.; Suzuki, N.; Yashiro, N.; Omoda, R.; Ko, D.-S.; Shiratsuchi, T.; Sugimoto, T.; Ryu, S.; Ku, J. H.; Watanabe, T.; Park, Y.; Aihara, Y.; Im, D.; Han, I. T. High-Energy Long-Cycling All-Solid-State Lithium Metal Batteries Enabled by Silver−Carbon Composite Anodes. *Nat. Energy* **2020**, *5*, 299−308.

(6) Xu, S.; McOwen, D. W.; Zhang, L.; Hitz, G. T.; Wang, C.; Ma, Z.; Chen, C.; Luo, W.; Dai, J.; Kuang, Y.; Hitz, E. M.; Fu, K.; Gong, Y.; Wachsman, E. D.; Hu, L. All-in-One Lithium-Sulfur Battery Enabled by a Porous-Dense-Porous Garnet Architecture. *Energy Storage Mater.* **2018**, *15*, 458−464.

(7) Park, K. H.; Bai, Q.; Kim, D. H.; Oh, D. Y.; Zhu, Y.; Mo, Y.; Jung, Y. S. Design Strategies, Practical Considerations, and New Solution Processes of Sulfide Solid Electrolytes for All-Solid-State Batteries. *Adv. Energy Mater.* **2018**, *8*, 1800035.

(8) Xu, R.; Yue, J.; Liu, S.; Tu, J.; Han, F.; Liu, P.; Wang, C. Cathode-Supported All-Solid-State Lithium−Sulfur Batteries with High Cell-Level Energy Density. *ACS Energy Lett.* **2019**, *4*, 1073−1079.

(9) Liang, Y.; Tao, Z.; Chen, J. Organic Electrode Materials for Rechargeable Lithium Batteries. *Adv. Energy Mater.* **2012**, *2*, 742−769.

(10) Song, Z.; Zhou, H. Towards Sustainable and Versatile Energy Storage Devices: An Overview of Organic Electrode Materials. *Energy Environ. Sci.* **2013**, *6*, 2280−2301.

(11) Liang, Y.; Yao, Y. Positioning Organic Electrode Materials in the Battery Landscape. *Joule* **2018**, *2*, 1690−1706.

(12) Hao, F.; Han, F.; Liang, Y.; Wang, C.; Yao, Y. Architectural Design and Fabrication Approaches for Solid-State Batteries. *MRS Bull.* **2018**, *43*, 775−781.

(13) Poizot, P.; Gaubicher, J.; Renault, S.; Dubois, L.; Liang, Y.; Yao, Y. Opportunities and Challenges for Organic Electrodes in Electrochemical Energy Storage. *Chem. Rev.* **2020**, *120*, 6490−6557.

(14) Heiska, J.; Nisula, M.; Karppinen, M. Organic Electrode Materials with Solid-State Battery Technology. *J. Mater. Chem. A* **2019**, *7*, 18735−18758.

(15) Koerver, R.; Aygün, I.; Leichtweiß, T.; Dietrich, C.; Zhang, W.; Binder, J. O.; Hartmann, P.; Zeier, W. G.; Janek, J. Capacity Fade in Solid-State Batteries: Interphase Formation and Chemomechanical Processes in Nickel-Rich Layered Oxide Cathodes and Lithium Thiophosphate Solid Electrolytes. *Chem. Mater.* **2017**, *29*, 5574−5582.

(16) Hao, F.; Chi, X.; Liang, Y.; Zhang, Y.; Xu, R.; Guo, H.; Terlier, T.; Dong, H.; Zhao, K.; Lou, J.; Yao, Y. Taming Active Material-Solid Electrolyte Interfaces with Organic Cathode for All-Solid-State Batteries. *Joule* **2019**, *3*, 1349−1359.

(17) Chi, X.; Liang, Y.; Hao, F.; Zhang, Y.; Whiteley, J.; Dong, H.; Hu, P.; Lee, S.; Yao, Y. Tailored Organic Electrode Material Compatible with Sulfide Electrolyte for Stable All-Solid-State Sodium Batteries. *Angew. Chem., Int. Ed.* **2018**, *57*, 2630−2634.

(18) Luo, C.; Ji, X.; Chen, J.; Gaskell, K. J.; He, X.; Liang, Y.; Jiang, J.; Wang, C. Solid-State Electrolyte Anchored with a Carboxylated Azo Compound for All-Solid-State Lithium Batteries. *Angew. Chem., Int. Ed.* **2018**, *57*, 8567−8571.
(19) Liang, Y.; Zhang, P.; Chen, J. Function-Oriented Design of Conjugated Carbonyl Compound Electrodes for High Energy Lithium Batteries. *Chem. Sci.* **2013**, *4*, 1330−1337.
(20) Zhu, Z.; Hong, M.; Guo, D.; Shi, J.; Tao, Z.; Chen, J. All-Solid-State Lithium Organic Battery with Composite Polymer Electrolyte and Pillar[5]Quinone Cathode. *J. Am. Chem. Soc.* **2014**, *136*, 16461−16464.
(21) Lécuyer, M.; Gaubicher, J.; Barrès, A.-L.; Dolhem, F.; Deschamps, M.; Guyomard, D.; Poizot, P. A Rechargeable Lithium/Quinone Battery Using a Commercial Polymer Electrolyte. *Electrochem. Commun.* **2015**, *55*, 22−25.
(22) Liang, J.; Li, X.; Zhao, Y.; Goncharova, L. V.; Wang, G.; Adair, K. R.; Wang, C.; Li, R.; Zhu, Y.; Qian, Y.; Zhang, L.; Yang, R.; Lu, S.; Sun, X. In Situ Li_3PS_4 Solid-State Electrolyte Protection Layers for Superior Long-Life and High-Rate Lithium-Metal Anodes. *Adv. Mater.* **2018**, *30*, 1804684.
(23) Tröltzsch, U.; Kanoun, O.; Tränkler, H.-R. Characterizing Aging Effects of Lithium Ion Batteries by Impedance Spectroscopy. *Electrochim. Acta* **2006**, *51*, 1664−1672.
(24) Han, F.; Zhu, Y.; He, X.; Mo, Y.; Wang, C. Electrochemical Stability of $Li_{10}GeP_2S_{12}$ and $Li_7La_3Zr_2O_{12}$ Solid Electrolytes. *Adv. Energy Mater.* **2016**, *6*, 1501590.
(25) Dewald, G. F.; Ohno, S.; Kraft, M. A.; Koerver, R.; Till, P.; Vargas-Barbosa, N. M.; Janek, J.; Zeier, W. G. Experimental Assessment of the Practical Oxidative Stability of Lithium Thiophosphate Solid Electrolytes. *Chem. Mater.* **2019**, *31*, 8328−8337.
(26) Koerver, R.; Walther, F.; Aygün, I.; Sann, J.; Dietrich, C.; Zeier, W. G.; Janek, J. Redox-Active Cathode Interphases in Solid-State Batteries. *J. Mater. Chem. A* **2017**, *5*, 22750−22760.
(27) Jung, S. H.; Kim, U.-H.; Kim, J.-H.; Jun, S.; Yoon, C. S.; Jung, Y. S.; Sun, Y.-K. Ni-Rich Layered Cathode Materials with Electrochemo-Mechanically Compliant Microstructures for All-Solid-State Li Batteries. *Adv. Energy Mater.* **2020**, *10*, 1903360.
(28) Li, X.; Ren, Z.; Norouzi Banis, M.; Deng, S.; Zhao, Y.; Sun, Q.; Wang, C.; Yang, X.; Li, W.; Liang, J.; Li, X.; Sun, Y.; Adair, K.; Li, R.; Hu, Y.; Sham, T.-K.; Huang, H.; Zhang, L.; Lu, S.; Luo, J.; Sun, X. Unravelling the Chemistry and Microstructure Evolution of a Cathodic Interface in Sulfide-Based All-Solid-State Li-Ion Batteries. *ACS Energy Lett.* **2019**, *4*, 2480−2488.
(29) Nagao, M.; Hayashi, A.; Tatsumisago, M. High-Capacity Li_2S−Nanocarbon Composite Electrode for All-Solid-State Rechargeable Lithium Batteries. *J. Mater. Chem.* **2012**, *22*, 10015−10020.
(30) Pu, K.; Qu, X.; Zhang, X.; Hu, J.; Gu, C.; Wu, Y.; Gao, M.; Pan, H.; Liu, Y. Nanoscaled Lithium Powders with Protection of Ionic Liquid for Highly Stable Rechargeable Lithium Metal Batteries. *Adv. Sci.* **2019**, *6*, 1901776.
(31) Lim, J.; Chong, M. S.; Chan, J. K.; Teoh, S. H. Polymer Powder Processing of Cryomilled Polycaprolactone for Solvent-Free Generation of Homogeneous Bioactive Tissue Engineering Scaffolds. *Small* **2014**, *10*, 2495−502.
(32) Choi, S.; Jeon, M.; Ahn, J.; Jung, W. D.; Choi, S. M.; Kim, J.-S.; Lim, J.; Jang, Y.-J.; Jung, H.-G.; Lee, J.-H.; Sang, B.-I.; Kim, H. Quantitative Analysis of Microstructures and Reaction Interfaces on Composite Cathodes in All-Solid-State Batteries Using a Three-Dimensional Reconstruction Technique. *ACS Appl. Mater. Interfaces* **2018**, *10*, 23740−23747.
(33) Bielefeld, A.; Weber, D. A.; Janek, J. Microstructural Modeling of Composite Cathodes for All-Solid-State Batteries. *J. Phys. Chem. C* **2019**, *123*, 1626−1634.
(34) Park, J.; Kim, K. T.; Oh, D. Y.; Jin, D.; Kim, D.; Jung, Y. S.; Lee, Y. M. Digital Twin-Driven All-Solid-State Battery: Unraveling the Physical and Electrochemical Behaviors. *Adv. Energy Mater.* **2020**, *10*, 2001563.
(35) Choi, H. U.; Jin, J. S.; Park, J.-Y.; Lim, H.-T. Performance Improvement of All-Solid-State Li-S Batteries with Optimizing Morphology and Structure of Sulfur Composite Electrode. *J. Alloys Compd.* **2017**, *723*, 787−794.
(36) Han, F.; Yue, J.; Fan, X.; Gao, T.; Luo, C.; Ma, Z.; Suo, L.; Wang, C. High-Performance All-Solid-State Lithium−Sulfur Battery Enabled by a Mixed-Conductive Li_2S Nanocomposite. *Nano Lett.* **2016**, *16*, 4521−4527.
(37) Huggins, R. A. Simple Method to Determine Electronic and Ionic Components of the Conductivity in Mixed Conductors a Review. *Ionics* **2002**, *8*, 300−313.
(38) Strauss, F.; Bartsch, T.; de Biasi, L.; Kim, A. Y.; Janek, J.; Hartmann, P.; Brezesinski, T. Impact of Cathode Material Particle Size on the Capacity of Bulk-Type All-Solid-State Batteries. *ACS Energy Lett.* **2018**, *3*, 992−996.
(39) Shi, T.; Tu, Q.; Tian, Y.; Xiao, Y.; Miara, L. J.; Kononova, O.; Ceder, G. High Active Material Loading in All-Solid-State Battery Electrode Via Particle Size Optimization. *Adv. Energy Mater.* **2020**, *10*, 1902881.

https://dx.doi.org/10.1021/acsenergylett.0c02227
ACS Energy Lett. 2021, 6, 201−207